Molecular mechanism and energetics of coupling between substrate binding and product release in the F₁-ATPase catalytic cycle

Michał Badocha[a] [ID], Miłosz Wieczór[a], Antoni Marciniak[a] [ID], Cyprian Kleist[a], Helmut Grubmüller[b,1] [ID], and Jacek Czub[a,c,1]

F₁-ATPase is a motor protein that couples the rotation of its rotary γ subunit with ATP synthesis or hydrolysis. Single-molecule experiments indicate that nucleotide binding and release events occur almost simultaneously during the synthesis cycle, allowing the energy gain due to spontaneous binding of ADP to one catalytic β subunit to be directly harnessed for driving the release of ATP from another rather than being dissipated as heat. Here, we examine the unknown mechanism of this coupling that is critical for an exceptionally high mechanochemical efficiency of F₁-ATPase by means of all-atom free-energy simulations. We find that nondissipative and kinetically fast progression of the motor in the synthesis direction requires a concerted conformational change involving the closure of the ADP-binding β subunit followed by the gradual opening of the ATP-releasing β subunit over the course of the 30 to 40° rotary substep of the γ subunit. This rotary substep, preceding the ATP-dependent metastable state, allows for the recovery of a large portion of the ADP binding energy in the conformation of ATP-bound β that gradually adopts the low-affinity conformation, captured also by the recent cryo-EM structure of this elusive state. The release of ATP from this nearly open conformation leads to its further opening, which enables the progression of the motor to the next catalytic metastable state. Our simulations explain this energy conversion mechanism in terms of intersubunit and ligand–protein interactions.

ATP synthase | motor proteins | bioenergetics | molecular dynamics

ATP synthase is an evolutionarily conserved multisubunit protein complex which utilizes the electrochemical proton gradient across energy-transducing membranes in mitochondria, chloroplasts, and bacteria to synthesize adenosine triphosphate (ATP) from adenosine diphosphate (ADP) and inorganic phosphate; however, at low proton motive force, it can also operate in reverse as an ATP-hydrolyzing proton pump (1, 2). Like other members of this enzyme family, ATP synthase is composed of two opposing rotary motors: the membrane-bound F₀, powered by proton translocation, and the hydrophilic ATP-driven F₁, mechanically coupled to F₀ by the rotating γ subunit (3, 4). In the synthesis mode, the torque generated by F₀ causes the asymmetric γ subunit of F₁-ATPase to rotate inside the catalytic headpiece comprising three alternating α and β subunits (Fig. 1) (2, 5–7). This rotation of the γ-shaft proceeds stepwise, in response to which the three catalytic sites located largely within the β subunits undergo cyclic transitions between conformations with different nucleotide affinities, ultimately leading to ATP synthesis even against cellular ATP: ADP concentration ratios that strongly favor hydrolysis (2, 5).

In single-molecule imaging experiments, it has been shown that each full hydrolytic or synthetic cycle in F₁-ATPase is completed with a 120° rotary step of the γ-shaft (5, 6, 8). At low ATP concentrations, these full steps were further resolved into 80 to 90° and 40 to 30° substeps which, in the hydrolysis direction, coincide with ATP binding and ATP hydrolysis, respectively, and thus correspond to transitions between two metastable states, referred to as the ATP-dependent and catalytic dwell states (9, 10). In mitochondrial F₁-ATPase, between these two states, at least one additional dwell state has been identified that is believed to precede the release of phosphate (or phosphate and ADP) (11–13).

The observed stepping pattern enables F₁-ATPase to convert the chemical free energy of ATP hydrolysis into mechanical work (and vice versa) with only very little heat dissipation, even relatively far from the quasistatic limit (14, 15). This remarkable, almost 100% efficiency of energy conversion, much higher than for a typical linear motor (16), requires that changes in the occupancy of the catalytic sites be tightly coupled to the concerted conformational transitions of the α₃β₃ hexamer and thereby to the mechanical steps of the γ-shaft. In particular, the energy gain due to

spontaneous ADP binding cannot be dissipated but has to be utilized as the synthetic cycle progresses. In fact, within the accuracy of single-molecule measurements, ADP binding occurs concomitantly with ATP release, at the angular position of γ corresponding to the ATP-dependent dwell (11, 12). This strongly suggests that ADP binding to one β subunit is harnessed for driving the release of ATP from the other, i.e., for the most energetically costly event in the synthesis direction (12, 17). Since product release is a rate-limiting process, its direct coupling to substrate binding is also critical for F_1 kinetic efficiency, as rapid hydrolysis has been shown to require coordination of the binding sites by the γ-shaft (18, 19). It has been predicted that at physiological ATP concentrations, ADP release is accelerated by about six orders of magnitude when it is coupled to the ATP-binding event in another β subunit (13).

To elucidate the molecular mechanism underlying this γ-mediated coupling, here, we use fully atomistic simulations of solvated F_1 with free-energy calculations. In recent years, by allowing to probe spatial and temporal scales that are difficult to access experimentally, molecular simulations have proven useful in explaining many aspects of the mechanism underlying ATP synthesis in F_1. In particular, the free-energy landscapes governing the rotary catalysis have been determined using a coarse-grained model of F_1 (20, 21) and, more recently, the related hexameric V_1-ATPase motor (22). These landscapes allowed us to describe general features of the mechanochemical coupling, including the structural and energetic determinants of the unidirectional stepwise rotation of the γ shaft and the generated torque as well as predicted the electrostatic nature of the energy conversion mechanism (20–22). Atomistic simulation approaches, given the time-scale limitations, focused on accurate descriptions of selected aspects of the mechanism, including the transmission of elastic energy (23, 24), the timing of phosphate release (25), and the response of the $\alpha_3\beta_3$ conformation to the rotary motion of the γ-shaft (26–29). Notably, thermodynamics and kinetics of conformational transitions in V_1 have also been studied at atomic resolution to provide a unified model of its simpler 120° stepping without substeps (30).

Recently, we have determined the free-energy landscape governing the main rotary substep of the mammalian F_1 during which the γ-shaft, initially oriented as in the so-called "ground-state" structure, with its convex side toward the empty β subunit (β_E), rotates by ~70° to reach a new metastable position in between β_E and β_{TP} (Fig. 1) (31). Consistently with structural and single-molecule data (11, 32), this rotation likely represents the transition to the ATP-dependent state that is responsible for harnessing the binding energy for product release.

Here, we show that nondissipative and fast progression to this dwell state requires closing of β_E and opening of β_{TP} to be strongly coupled. Since in the synthesis cycle, these conformational changes are associated with ADP binding and ATP release, respectively (3, 33), our results explain the coordination between these chemical events and how they are coupled to the mechanical rotation of γ. We also analyze the transition to the ATP-dependent dwell and subsequent ATP release in structural and energetic terms to provide an atomic-level understanding of how the motor minimizes futile expenditure of energy.

Results and Discussion

Closing Transition of β_E Drives Rotation of the γ-Shaft that Is Opposed by β_{TP}. ATP release from β_{TP} in the synthetic cycle is thought to occur at the angular position of γ in the range of 60 to 90°, with respect to the "ground state" crystal structure ($\theta = 0°$, *SI Appendix*, Fig. S1), in which the convex side of γ faces β_E in the open conformation (red in Fig. 1 *A* and *B*) (11, 32). Therefore, to understand the interplay between the γ-shaft progression, ATP release, and ADP binding, we computed the free-energy landscape, $G(\theta)$, which governs the rotation of γ from 60° up to the final state at 120°, where γ faces the (now empty) β_{TP} concluding one synthetic cycle (Fig. 1 *A* and *B* and Movie S1). It is commonly accepted that the release of ATP from β_{TP} is associated with its transition from the closed state (T_C) to the open state (T_O), while ADP binding to β_E causes its reverse conformational change, from E_O to E_C (Fig. 1) (3, 33).
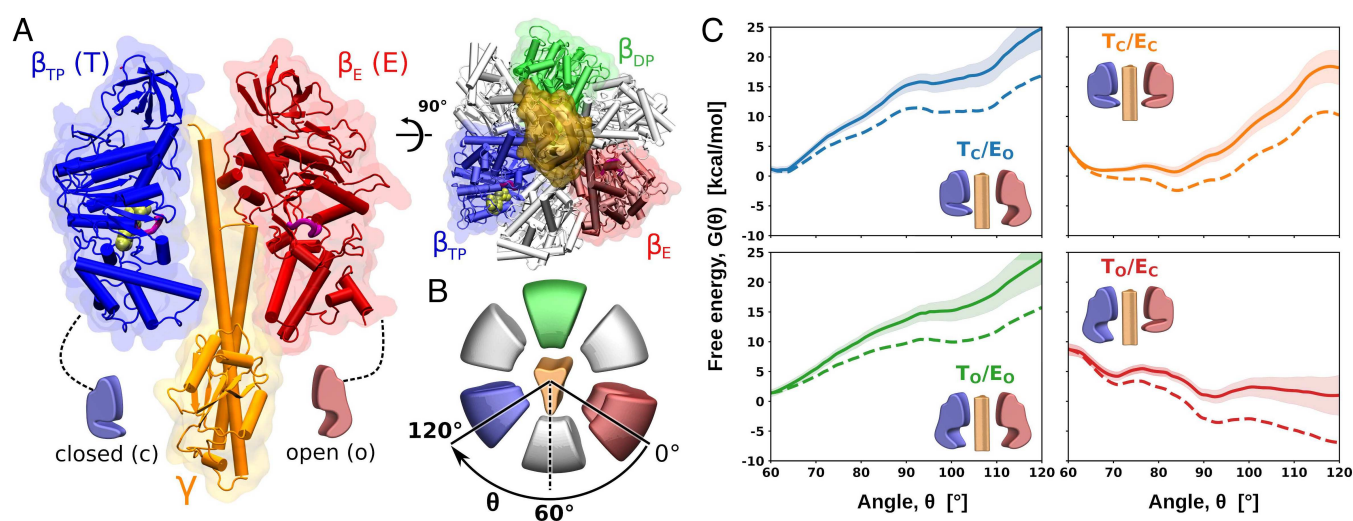
Fig. 1. (*A*) Structure of F_1-ATPase. For clarity, the sideview (*Left*) shows only two β subunits, β_E (red) and β_{TP} (blue), involved in ADP binding and ATP release, respectively, in a single synthesis cycle. The convex side of the γ-shaft (orange) faces the α subunit located between β_E and β_{TP}, which corresponds to the angle $\theta = 60°$. (The opposite view is depicted in *SI Appendix*, Fig. S2.) Consistently with their occupancy state, the ATP-bound β_{TP} and empty β_E assume the closed and open conformations, respectively. (*B*) Definition of the rotation angle θ. (*C*) Free energy as a function of the rotation angle θ at different conformational states of β_E (E) and β_{TP} (T) (solid lines); c denotes closed, and o denotes open. The shaded areas indicate statistical uncertainties of the free energies. Dashed lines show the free-energy profiles modified by adding the F_O-generated torque potential with a constant slope of −0.13 kcal/° (34).

To examine the putative coupling between γ progression to the open/close conformational changes of the β_E and β_{TP} subunits, we decided to artificially remove any coupling in our simulations and to study the energetics of the individual conformational changes separately. In a first step, the free-energy profiles for the $60 \rightarrow 120°$ rotation were determined for all four conformational state combinations of β_{TP} and β_E (T_CE_O, T_CE_C, T_OE_O, T_OE_C). In each of the four free-energy simulations, the two β subunits were kept in their open or closed conformations with a potential preserving conformational flexibility (Fig. 1C). We employed the well-established umbrella sampling method to determine the free-energy profiles and ran the simulations extensively until convergence, as evidenced in *SI Appendix*, Fig. S3 in which the free-energy values no longer change with added simulation time.

The four resulting free-energy profiles in Fig. 1C are strikingly different from each other, revealing that, in the $60 \rightarrow 120°$ range, rotation energetics strongly depends on the conformational state of the two involved catalytic subunits. Most importantly, the steep energy increase (by ~3.5 kcal/mol per $10°$) observed for both T_CE_O and T_OE_O shows that when β_E remains open, the rotation is strongly inhibited. This holds true even when the motor is driven by an F_o-generated external torque (dashed lines in Fig. 1C). In fact, for the γ shaft to proceed efficiently beyond $60°$, β_E has to close, which completely eliminates the free-energy barrier (T_CE_C and T_OE_C in Fig. 1C). This dependence provides evidence for tight coupling between ADP binding and rotation in the synthesis direction. However, if the closure of β_E at $60°$ occurs in the presence of open β_{TP} (T_OE_C), the γ-shaft unexpectedly proceeds "downhill" in free energy up to $90°$. This indicates that in the T_OE_C conformational state, the rotation would be spontaneous in the synthesis direction and thus the energy gain due to ADP binding would largely be dissipated through the rotary motion of γ. On the contrary, when β_{TP} remains closed (T_CE_C in Fig. 1C), the profile from $60°$ up to $90°$ is much flatter, showing that the closed conformation of β_{TP} exerts an opposing force to rotating γ. This allows for harnessing the mechanical energy of γ, otherwise dissipated as heat, to drive the transition of β_{TP} to its low-affinity open state. By subtracting the T_CE_C and T_OE_C free-energy changes in the $60 \rightarrow 90°$ range, we can roughly estimate the upper bound of this energy stored back in β_{TP} to be 4.5 kcal/mol, which is quite consistent with the free energy of ADP binding to the isolated β subunit at physiological conditions, e.g., -4 kcal/mol (35). Finally, comparison of the T_CE_C profile displaying a rapid free-energy increase in the $90 \rightarrow 120°$ range with the T_OE_C profile, almost flat in this region, suggests that the rotation beyond $90°$ occurs only after opening of β_{TP} and hence only after ATP release.

Taken together, our first set of free-energy profiles suggests a tight coupling mechanism between ADP binding and ATP release mediated by the rotation of the γ-shaft, which proceeds as follows: 1) Prior to $60°$, ADP binds to β_E which then helps to drive rotation of γ up to $\sim90°$, accompanied by a gradual opening of β_{TP} that allows recovery of a large portion of the ADP binding energy in the conformation of ATP-bound β_{TP}. 2) Near $90°$, corresponding to the actual ATP-dependent metastable state, ATP is released from β_{TP} that leads to its full opening, which in turn enables further progression of γ toward $120°$. The resulting free-energy landscape governing the motion of γ inside the $\alpha_3\beta_3$ headpiece is almost flat in the entire $60 \rightarrow 120°$ range (*SI Appendix*, Fig. S4). This means that the metastable states involved have nearly the same free energy, and thus, very little energy is lost during these substeps, accounting for the known high thermodynamic efficiency of the energy conversion in F_1.

The lack of pronounced activation barriers to rotation in the calculated landscape, in turn, underlies high catalytic turnover when F_1 is driven by F_o or by ATP hydrolysis.

Importantly, the above scenario implies the existence of an extra ADP-dependent metastable state (i.e., the ADP-waiting dwell in the synthesis mode) that precedes the ATP-dependent dwell by $\sim30°$ (or more). This prediction is in a very good agreement with a recent reanalysis of the single-molecule data that revealed a new short-lived metastable intermediate at $36°$ before the ATP-dependent dwell (in synthesis mode) (13).

Intersubunit Electrostatic Interactions Complemented by Steric Repulsion Mediate the Coupling Between β_E/β_{TP} Conformation and γ Rotation. Next, we examined the structural determinants of the above coupling mechanism. Specifically, we asked how the closure of β_E can drive the rotation of γ beyond $60°$ and which intersubunit interactions allow for subsequent conversion of the rotational energy into the conformational energy of ATP-bound β_{TP}.

Aiming at a qualitative answer to these questions, we calculated the number of contacts between the γ-shaft and either β_E or β_{TP} as a function of the rotation angle θ for all four conformational states of β_{TP} and β_E (T_CE_O, T_CE_C, T_OE_O, and T_OE_C). We found (*SI Appendix*, Fig. S5 and Movie S2) that even though the total number of γ/β_E contacts is largely independent of the conformational state, the specific contact pattern differs markedly between the four states. In particular, the closure of β_E decreases the number of contacts between the inner loops of its central domain (residues R279–P287 and I314–D323 and the α-helical coiled coil in γ (*SI Appendix*, Fig. S6)), while, at the same time, it increases the contact area between the β_E C-terminal domain and the upper face of the globular domain of γ (*SI Appendix*, Figs. S5 and S6). Because the latter two surfaces are oppositely charged (*SI Appendix*, Fig. S7), the electrostatic attraction between them could, in fact, be a major factor in driving the $60 \rightarrow 90°$ rotation upon closure of β_E.

To test this hypothesis, we evaluated the relative contributions of all individual charged residues at the γ/β_E interface to the free-energy change upon the F_1 rotation from $\theta = 60°$ to $\theta = 90°$. For this purpose, we estimated how the derivative of the free-energy profile $G(\theta)$ with respect to the absolute value of the formal charge on the i-th side chain, q_i, changes between $60°$ and $90°$, $\Delta g_i = \partial G_{90°}/\partial q_i - \partial G_{60°}/\partial q_i$ (*Methods* for details). Accordingly, negative values of Δg_i indicate residues that upon further charging promote the $60 \rightarrow 90°$ rotation, and vice versa. To extract the effect of the closing transition of β_E on the rotation of γ, in Fig. 2A, we show the differences in Δg_i between the systems differing only in the conformation of β_E, i.e., T_CE_C and T_CE_O, and denote them as $\Delta\Delta g_i$.

As can be seen in Fig. 2A and *SI Appendix*, Fig. S8, many residues characterized by negative $\Delta\Delta g$ are found particularly in the upper face of the globular domain of γ (e.g., R75, R133, and R228) and, to a lesser extent, in the conserved DELSEED loop of the β_E C-terminal domain (e.g., E403 and E404), which has been previously found to participate in the energy transduction in F_1 (36). This suggests that closing of β_E indeed allows for more favorable electrostatic interactions between these two regions. Consistently, the analysis of the electrostatic potential around γ and β_E shows that when β_E is closed, the attractive interaction between the two charged surfaces is greatly enhanced in response to the $60 \rightarrow 90°$ rotation (Fig. 2B). Furthermore, the N-terminal portion of the coiled coil (e.g., R8, R9, and K11) and the upper helix of the C-terminal domain of β_E (e.g., D390 and K386) also
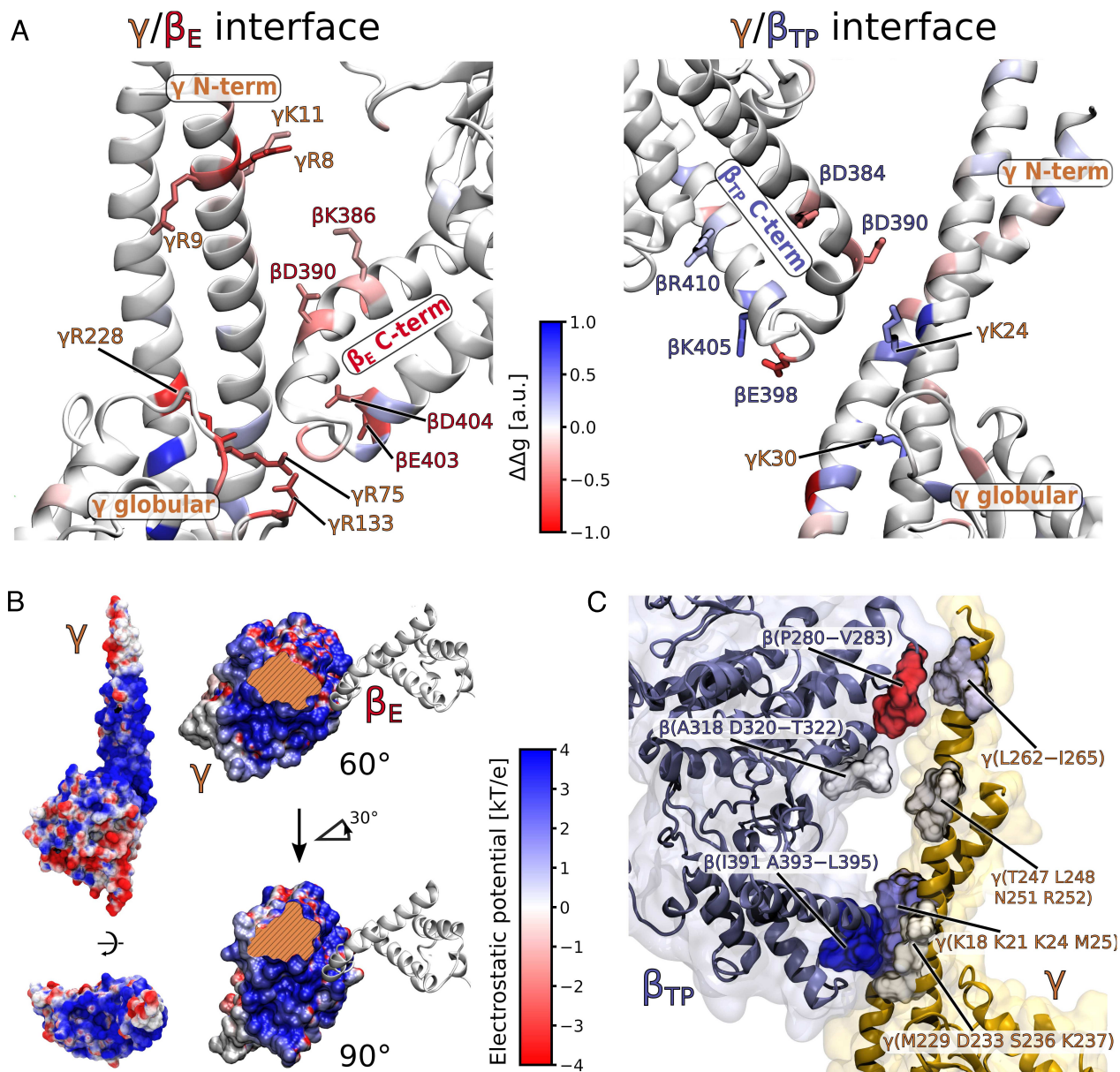
Fig. 2. (*A*) Effect of the closing transition on the relative contributions of all charged residues at the γ/β_E and γ/β_{TP} interfaces to the free-energy change upon the 60→90° rotation of the γ-shaft. The values of $\Delta\Delta g_i$ (see definition in the text) are color-coded onto the F₁ structure such that the residues whose charging promotes the 60→90° rotation in the closed state more than in the open are shown in red (negative $\Delta\Delta g_i$), and those hindering the rotation are in blue (positive $\Delta\Delta g_i$). Labels of all residues are provided in *SI Appendix*, Fig. S8. (*B*) Electrostatic potential pattern on the molecular surface of the γ subunit of F₁. The *Right* panel (*Top* view) shows how the 60→90° rotation of γ facilitates the interaction between the positively charged patch on the upper face of the globular domain of γ with the negatively charged C-terminal domain of β_E. (The distribution of the electrostatic potential on the surface of β_E is shown in *SI Appendix*, Fig. S7). (*C*) Effect of the closing transition on the relative contribution of van der Waals interactions between the γ-shaft and β_{TP} at the three regions of contact between them to the free-energy change upon the 60→90° rotation. Analogously to panel *A*, blue values of $\Delta\Delta g_i$ denote regions whose increased molecular volume opposes the rotation more in the closed than in the open state of β_{TP} and vice versa.

seem to favor the rotation of γ, as indicated by negative $\Delta\Delta g$ in Fig. 2*A*.

Overall, we find that the attraction between the positively charged regions in the globular and coiled coil domains of γ and the negatively charged C-terminal domain of β_E provides a possible electrostatic mechanism by which ADP-induced closing of β_E can drive the rotation of γ from 60 to 90°. More generally, this finding adds to an accumulating body of research pointing to a dominant role for electrostatics in the mechanochemical coupling of F₁-ATPase and related motors (20, 21, 30, 31).

In contrast, the same analysis focused on the γ/β_{TP} interface (Fig. 2*C*) does not provide a clear electrostatics-based picture

of the energy transmission between the rotating γ and the ATP-bound β_{TP}. On the one hand, the lower helix of the β_{TP} C-terminal domain (that has a net cationic charge, e.g., R410 and K405; *SI Appendix*, Fig. S7) indeed seems to oppose the 60→90° rotation more effectively in the closed than in the open state (positive $\Delta\Delta g$), presumably by repulsion with the convex region of the γ coiled coil (e.g., K30 or K24). This interaction could therefore play a role in the γ-mediated opening of the β_{TP}, at the same time, providing a possible molecular explanation for mutagenesis results showing that neutralization of positively charged residues in this helix decouples rotation and chemical events (37, 38). On the other hand,

however, electrostatic interactions involving the upper helix of the C-terminal domain (e.g., D384 and D390) and, to a lesser degree, the DELSEED loop (e.g., E398) promote the rotation (negative $\Delta \Delta g$) and thus cannot participate in converting the γ mechanical energy into the conformational energy of β_{TP}.

Another hint that the opening of β_{TP} cannot be explained solely by electrostatic forces comes from the comparison of the intersubunit contact patterns between the systems $T_C E_C$ and $T_C E_O$, which reveals that upon closure of β_E, the number of contacts between γ and β_{TP} increases ~3 times (*SI Appendix*, Fig. S5 and Movie S2). The fact that closing β_E pushes γ toward β_{TP} suggests that steric interactions might also play a major role in the rotation-induced opening of β_{TP}. To test this notion, we used the same procedure as before, except that the derivatives were computed with respect to the atom size (σ parameter in the Lennard-Jones potential), and the analysis was focused on the three regions of contact between the γ-shaft and β_{TP} (Fig. 2C). Indeed, it can be seen that positive values of $\Delta \Delta g$ are found especially for the middle section of the γ N-terminal helix and the upper part of the β_{TP} DELSEED loop, i.e., the regions that are in direct contact throughout the $60 \rightarrow 90°$ rotation. This means that for closed β_{TP}, the growing van der Waals volume of these regions disfavors the rotation more noticeably than for open β_{TP}. We thus conclude that steric repulsion between γ and the C-terminal domain of β_{TP} may indeed contribute markedly to the opening of β_{TP} in response to the $60 \rightarrow 90°$ rotation. The importance of steric effects is in line with and explains recent studies that found, by measuring the effect of glycine and alanine substitutions on the generated torque, that conformational rigidity of the DELSEED loop rather than its charge might be essential for the F_1 mechanochemical efficiency (39).

The Release of ATP from β_{TP} Is Preceded by the Transition to the Nearly Open Conformation. In the mechanism suggested by our free-energy profiles (Fig. 1C), the $60 \rightarrow 90°$ rotation of the γ-shaft, triggered and partially driven by ADP binding to β_E, leads to gradual transition of β_{TP} to its low-affinity open state. This allows for harnessing the mechanical energy of γ for the release of ATP, the costliest event during the synthesis cycle (12, 17).

To directly test this energy conversion mechanism and to further disentangle the coupling between the γ-shaft and the two involved β subunits, we performed a second set of free-energy calculations. In these, we kept the γ subunit fixed and investigated how the free-energy landscape for the β conformational change depends on the position of the γ subunit. Specifically, we calculated the free energy as a function of the conformational coordinate describing the opening transition of β_{TP} (*Methods* for details) for three different angular positions of γ: 0, 60, and 90°.

It can be seen in Fig. 3A that, when γ faces β_E at 0°, β_{TP} assumes the closed conformation found in the ground-state F_1 crystal structure, as indicated by the well-pronounced free-energy minimum at -2.6 nm. In fact, this conformation is even more closed than the one observed for ATP-bound β_{TP} in the absence of the γ subunit, both in F_1 lacking γ (dashed line with the minimum at -1.8 nm) and in the isolated $\alpha\beta$ heterodimer (dot-dashed line). This additional stabilization of the closed conformation of β_{TP} in the complete F_1 is mostly due to interaction with the globular portion of γ that prevents the β_{TP} C-terminal domain from swinging outward (*SI Appendix*, Fig. S1) (28). However, when γ is rotated by 60° in the synthesis direction, its coiled coil portion exerts electrostatic and steric force onto
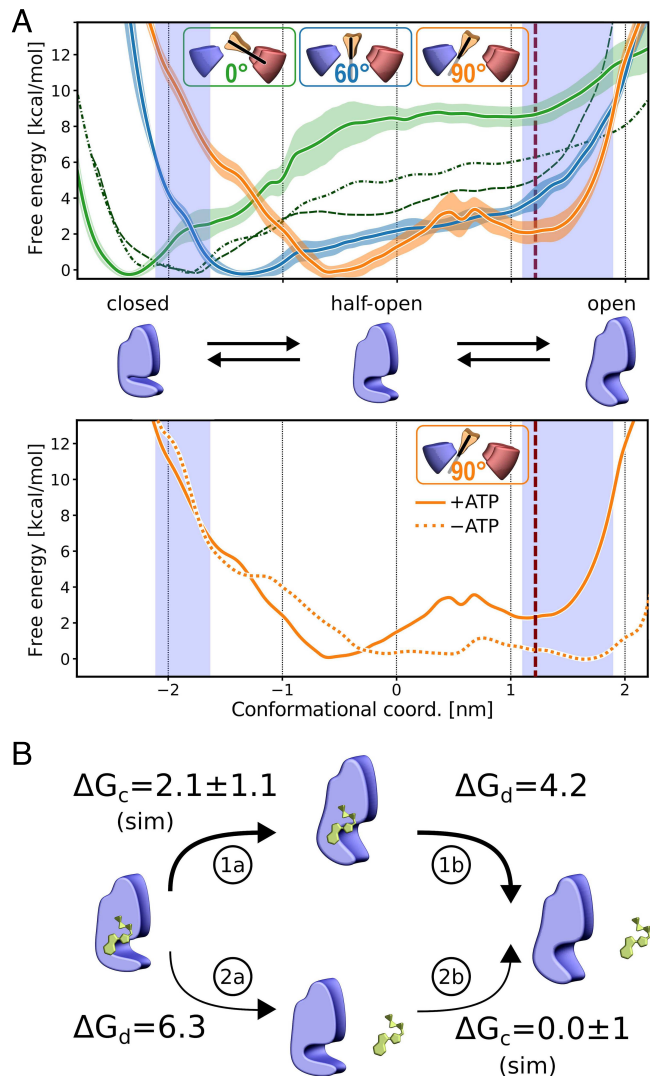

Fig. 3. (*A*) Free-energy profile governing the conformational dynamics of the ATP-bound β_{TP} subunit for the three different angular positions of the γ-shaft in the full F_1 complex: 0 (green), 60 (blue) and 90° (orange). Additionally, dashed and dash-dotted lines show the corresponding profiles for the ATP-bound β_{TP} in F_1 lacking the γ subunit ($\alpha_3\beta_3$ subcomplex) and in the isolated $\alpha\beta$ heterodimer, respectively. Conformational coordinate is the position along the vector connecting the centers of the closed and open states of β in the space spanned by all C_α atoms. The shaded blue regions show the extent of fluctuation of the conformational coordinate for the closed ATP-bound β_{TP} and the open nucleotide-free β_E as observed in the unbiased simulation of the $\alpha_3\beta_3$ subcomplex. The dashed dark red vertical line indicates the value of the conformational coordinate for the ATP-bound β_{TP} in the recent cryo-EM structure of bacterial F_1 in the ATP-dependent state (32). The *Bottom* panel shows the comparison of the conformational free-energy profiles for ATP-bound (solid) and nucleotide-free (dotted) β_{TP} in the ATP-dependent metastable state of the full F_1 ($\theta = 90°$). (*B*) Two limiting pathways of ATP release from β_{TP} in the ATP-dependent metastable state of F_1 ($\theta = 90°$): 1—the half-open β_{TP} undergoes the transition to the low-affinity nearly open conformation (1a) from which ATP subsequently dissociates (1b); 2—ATP dissociates directly from the half-open β_{TP} (2a), which is followed by the opening transtion (2b). The corresponding free-energy changes (in kcal/mol) for the conformational transitions (ΔG_c; 1a and 2b) are taken from our simulations (panel *B*); since the overall free-energy change for the ATP release at the γ position corresponding to the ATP-dependent dwell was measured to be 6.3 kcal/mol (12), we estimated the free energies for the dissociation steps (ΔG_d; 1b and 2a) by subtracting ΔG_c values from the experimental value.

β_{TP}, shifting its conformational equilibrium toward the open structure (the minimum in Fig. 3A moves to -1.4 nm). Consistent with the energy conversion mechanism proposed above, further 30° rotation of γ to the presumable ATP-dependent

dwell at 90° stores additional conformational energy within β_{TP} that opens up even more to reach the half-open state with its main minimum located around −0.5 nm.

Notably, at 90°, a new local free-energy minimum occurs at 1.2 nm, indicating that β_{TP} can occasionally (with probability of ∼3%) adopt a largely open conformation that is by 2.1 kcal/mol less stable than the dominant half-open state. In fact, this additional conformation closely matches (with the average C_α-RMSD of 0.22 nm) the conformation of β_{TP} in the ATP-dependent dwell, likely captured by the recent cryo-EM structure of F_1 from Bacillus PS3 (see the vertical dashed line in Fig. 3A and *SI Appendix*, Fig. S9 for structure superposition) (32). Since this conformation largely overlaps with the open state of β in the $\alpha_3\beta_3$ subcomplex (1.5 nm in Fig. 3A), while being slightly less open than the γ-induced open state of β_E in F_1 at 0° (2.3 nm), it will be referred to as "nearly open."

As discussed above, our rotation free-energy profiles in Fig. 1C indicate that the progression of γ beyond 90° requires opening of β_{TP}. However, from the conformational free-energy landscape at 90° (Fig. 3A), it is clear that ATP-bound β_{TP} prefers to remain mostly half open. This explains why ATP must be released at ∼90° for further γ subunit rotation beyond the ATP-dependent dwell.

To study the energetics and mechanism of ATP release from β_{TP} during the synthesis cycle, we extracted the thermodynamic cycle describing the possible limiting pathways for this process (Fig. 3B) from the above two sets of free-energy calculations (Figs. 1C and 3A). The experimentally determined free energy of ATP release in the ATP-dependent dwell of the bovine F_1 (ΔG_r) is ∼6.3 kcal/mol (at physiological ATP concentration) (12); however, it characterizes the overall process involving both the dissociation and conformational change events. Thus, to break down ΔG_r into these two free-energy components, one corresponding to ATP dissociation (ΔG_d) and the other corresponding to the β_{TP} conformational change (ΔG_c), we again calculated the conformational free-energy landscape of β_{TP} at 90°, but this time in the absence of bound ATP; the two landscapes are compared in the lower panel of Fig. 3A. It can be seen that without ATP, the nearly open conformation of β_{TP} shifts further by ca 0.6 nm toward the fully open state, and now, it becomes easily accessible and populated as the free energetic cost of the transition from half-open to nearly open conformation, ΔG_c, is reduced from 2.1 kcal/mol to roughly zero. Since in the absence of ATP, the half-open and nearly open states have very similar free energies (step 2b in Fig. 3C), it is clear that the dissociation of ATP directly from the half-open conformation (step 2a) is strongly disfavored ($\Delta G_d \approx \Delta G_r = 6.3$ kcal/mol). In contrast, the alternative pathway, i.e., transition to the nearly open state in the presence of ATP (step 1a), is preferred by ∼4 kcal/mol and occurs without any major activation barrier (Fig. 3B).

Therefore, taken together, we can conclude that the release of ATP during the synthetic cycle proceeds predominantly via pathway 1, i.e., the transition of β_{TP} to the nearly open state (step 1a with $\Delta G_c = 2.1$ kcal/mol) occurs first and is followed by the dissociation of ATP (1b) with $\Delta G_d = 4.2$ kcal/mol and a higher k_{off} rate compared to the dissociation directly from the half-open state (40). Finally, ATP dissociation leads to further opening of the nearly open β_{TP}, as indicated by Fig. 3B, triggering the next rotary substep from the ATP-dependent dwell at 90° to the catalytic dwell. Complete opening of the β_{TP} in the post–ATP-release state supports the conclusions of the previous single-molecule FRET experiments that found β_{TP} to be fully open in the ATP-waiting dwell of the hydrolysis cycle. According to

our current data, the two remaining β subunits in this dwell are closed; however, since we did not determine for them the full conformational energy landscape, we cannot exclude the possibility that one of them is in fact only half-closed as proposed by the FRET study (41).

γ-Induced Deformation of the Binding Site in the Nearly Open β_{TP} Drives ATP Release by an Electrostatic Mechanism.

As we have discussed above, when the γ-shaft progresses toward 90°, its rotational energy is converted into conformational energy of the ATP-bound β_{TP}, which itself is forced to open, eventually reaching the nearly open conformation at the ATP-dependent dwell. To understand how this energy input is used to drive ATP release from the nearly open conformation, we first examined the spatial distribution of elastic energy within β_{TP} in its nearly open state imposed by the γ-shaft held at 90°. To this end, we approximated the (effective) elastic energy as a function of individual backbone (ϕ and ψ) and side chain (χ) torsion angles, by Boltzmann-inverting their equilibrium distributions in the closed conformation of β_{TP}, treated as the relaxed reference state. Then, the average elastic energy stored in a given torsion angle due to the force applied by γ was computed as the expectation value over the distribution of this angle in the nearly open state. (Details are provided in *SI Appendix, Methods*).

In Fig. 4A, the average ϕ, ψ, and χ_1 elastic energies were added together and mapped onto the structure of β_{TP} in the nearly open conformation. As can be seen, in response to force applied by γ, the C-terminal portion of β_{TP} swings outward in a fairly rigid manner, which leads to accumulation of elastic energy mostly in the central nucleotide-binding domain. The structural elements of β_{TP} that become particularly conformationally strained are the H1 helix and the central part of the β-sheet (strands S3, S4, and S5), which form the binding site together with helix H2 and the P-loop (Fig. 4 A and B). Induced transition of β_{TP} to the nearly open state causes the H1 helix to change its orientation with respect to H2 from almost parallel to inclined and to approach the P-loop that is the phosphate recognition site. A substantial amount of energy stored in the β-sheet, when it becomes flatter during the opening transition, is consistent with the previous model, according to which the β-sheet plays the role of a "spring" mediating the energy transfer between γ and the binding site (42, 43).

To examine how the observed elastic deformation of the binding site might result in a decreased affinity for ATP, we calculated the change in the ATP-protein interaction energy (ΔE) when β_{TP} undergoes a transition from the closed to nearly open state and decomposed it into per-residue contributions (Fig. 4C). We found that the overall ΔE is dominated by the electrostatic interactions involving the triphosphate moiety. Specifically, the reorientation of H1 and, to a lesser extent, the flattening of the β-sheet lead to a significant weakening of attractive interactions with the highly conserved (*SI Appendix*, Fig. S10) arginine residues (R193, R195, and R264) that move away from ATP, as speculated previously (26). At the same time, and unexpectedly, the conserved negatively charged acidic residues located at the bottom surface of H1 (D199, E203, and E206) approach the P-loop–bound triphosphate, also contributing to lowering of the affinity. These changes are only partially compensated by a decrease in the repulsion with E192 and D260 and by the opposite-sign interactions involving the Mg^{2+} (Fig. 4C). In particular, the transition to the nearly open conformation makes the interaction between Mg^{2+} and H1 as well as R264 significantly more favorable. However, its effect on
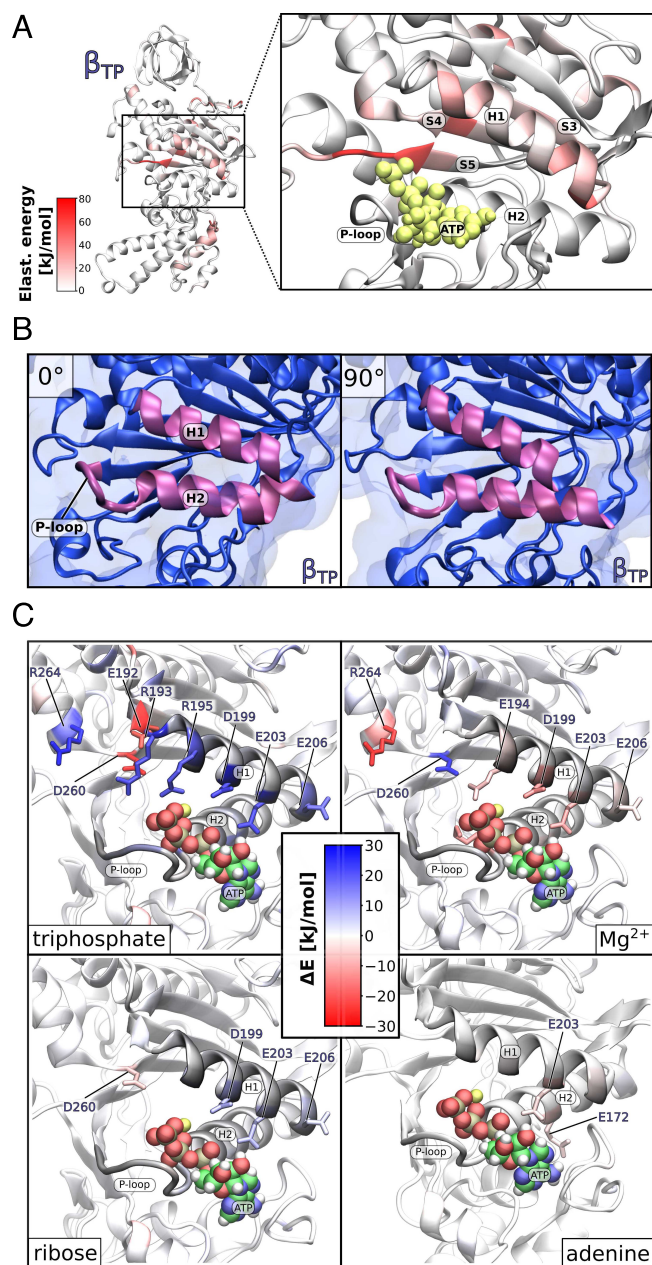
Fig. 4. (*A*) Distribution of elastic energy within the ATP-bound β_{TP} subunit in its nearly open conformation induced by the γ-shaft in the presumable ATP-dependent dwell (i.e., at 90°). The nucleotide-binding site is formed by the P-loop, helices H1 and H2, and the central region of the β-sheet (strands S3, S4, and S5). (*B*) Rotation of γ from 0 to 90° causes β_{TP} to undergo the transition from the closed conformation with almost parallel arrangement of the helices H1 and H2 (*Left*) to the nearly open conformation in which H1 and H2 align at an angle of about 30°, and the bottom negatively charged surface of H1 approaches the P-loop (*Right*). (*C*) Change in the interaction energy between different parts of ATP (triphosphate, Mg^{2+}, ribose, and adenine) and the β_{TP} subunit upon its γ-induced transition from the closed to the nearly open conformation. The total binding energy is decomposed into per-residue contributions that are mapped on the β_{TP} structure. A comparison of ATP-binding modes in the closed and nearly open β_{TP} is provided in *SI Appendix*, Fig. S11.

the repulsion with R193 and R195 is much less pronounced such that the net favorable enthalpic gain due to interactions involving Mg^{2+} does not outweigh the unfavorable change calculated for the triphoshpate. Enthalpic contributions to the binding affinity due to the adenine and ribose moieties are an order of magnitude smaller (Fig. 4*C*).

Conclusions

The exceptionally high mechanochemical efficiency of F$_1$-ATPase (14, 15) requires the free-energy gain due to ADP binding to be nearly fully utilized during the synthesis cycle rather than being dissipated as heat. Indeed, single-molecule experiments suggest that ADP binding and ATP release occur roughly synchronously, suggesting that spontaneous binding of the substrate to one β subunit (β_E) is tightly coupled to—and thus drives—the energetically costly release of the previously synthesized product from the neighboring β (β_{TP}) (12, 17).

To unveil the so-far unknown mechanism of this coupling, mediated by the rotary γ-shaft, we characterized the relevant conformational transitions of the beta and γ subunits as well as their mutual coupling, though extensive atomistic molecular dynamics free-energy calculations involving the fully solvated complete F1 part. In particular, we determined how the free-energy landscape underlying the rotation of F$_1$ in the angular range encompassing the ATP-dependent dwell depends on the conformational state of β_E and β_{TP}. We found that an energetically accessible and nondissipative pathway for the γ-shaft progression in this range involves a concerted conformational change consisting of the closure of β_E (at 60° or earlier) and the subsequent opening of β_{TP} at 90° (*SI Appendix*, Fig. S12 for a schematic depiction). This finding, augmented with the results of additional free-energy simulations of the angle-dependent conformational dynamics of β_{TP}, suggests a mechanism according to which, first, ADP binds to β_E, causing its closure which in turn triggers and partly drives the rotation of γ up to ~90°. This rotary substep allows for the recovery of a large portion of the ADP binding energy in the conformation of ATP-bound β_{TP} that gradually opens up. Next, at the 90° position, corresponding to the actual ATP-dependent dwell, ATP is released from β_{TP} following its transition to the nearly open conformation, as has recently been also captured by a new cryo-EM structure of this dwell (32). The release itself is driven by the deformation of the binding site that disturbs mainly electrostatic interactions involving attractive and repulsive forces between the triphosphate moiety and highly conserved charged amino acid residues. After ATP release, the nearly open conformation of β_{TP} is stabilized and opens up further, which triggers the rotation of the γ-shaft to the next catalytic dwell.

Importantly, the free-energy landscape governing the rotary substeps of γ in the above mechanism is nearly flat. On the one hand, this means that during these substeps, there is almost no wasteful dissipation of energy, explaining in part the high thermodynamic efficiency of F$_1$-ATPase. On the other, the lack of major free-energy barriers to rotation contributes to the rapid catalytic turnover. Our free-energy calculations also indirectly revealed a metastable state, related to ADP binding (or unbinding in the hydrolysis direction), postulated recently based on the reanalysis of single-molecule data (13, 44).

Finally, our analysis of intersubunit interactions in F$_1$ demonstrated that the rotary substep preceding the ATP-dependent dwell is governed by ADP-induced closure of β_E driven mainly by electrostatic attraction between the positively charged regions in the globular and coiled coil domains of γ and the negatively charged C-terminal domain of β_E. In contrast, the energy transmission between rotating γ and β_{TP} is mediated by a more complex combination of electrostatic and steric interactions.

Materials and Methods

Simulation Models and Molecular Dynamics Protocol. The initial configuration of the F$_1$ complex was extracted from the 2.3 Å crystal structure

(PDB entry 2JIZ) (45). Nucleotide ligands (ATP·Mg in β_{TP} and all three α subunits and ADP·Mg in β_{DP}) were kept, while the inhibitor (resveratrol) was removed from its binding site. The missing residues in the solvent-exposed part of the γ-subunit were added using our previous model based on the 1E79 crystal structure (46). To this end, we superimposed the complete structure of γ extracted from the previous model (31) on γ in 2JIZ and then transferred the coordinates of the missing residues to the model, while keeping the remaining part of γ, including the interface with the $\alpha_3\beta_3$ hexamer, unchanged. The protein and bound nucleotides were modeled using the CHARMM36 force field (47) and solvated with 100126 TIP3P water molecules in a rectangular 16.4 × 14.4 × 14.4 nm box. Then, 359 potassium and 313 chloride ions were added to neutralize the system at a physiological concentration of 0.15 M. Additionally, two other systems were prepared containing either the $\alpha_3\beta_3$ subcomplex or the ATP-bound $\alpha\beta$ heterodimer. To this end, we removed either only the γ subunit or all subunits except for α_{TP} and β_{TP}, respectively, from the F$_1$ system. The number of ions was adjusted accordingly to maintain electrical neutrality of the system. A temperature of 300 K was maintained with a Nosé–Hoover thermostat with a time constant of 0.5 ps, while a Parinello–Rahman barostat kept the pressure at 1 atm with a time constant of 2 ps. Bond lengths were constrained using the LINCS algorithm (48) for the protein and SETTLE (49) for water, allowing the use of a standard 2-fs timestep. The particle mesh Ewald (PME) method was used for electrostatics, with a short-range cutoff of 1.0-nm and 0.12-nm Fourier spacing (50). All simulations were performed using the Gromacs suite (51).

For all enforced rotation simulations, the flex2 functional form of the potential was used (52); the rotation was performed around the axis parallel to the x-dimension (longer side of the box), and the six N-terminal residues of the β subunits were harmonically restrained to their initial positions to mimic the immobilization effect of the peripheral stalk.

Rotation Free-Energy Landscape. To prepare the initial configurations for the combinatorial sampling of all four conformational states of subunits β_E and β_{TP}, the desired conformations were first enforced using a distance root mean square deviation (DRMSD)-based restraint over 750 ns in four separate steered MD simulations, with the crystal-structure β-subunit geometries from the PDB entry 2JIZ used as a reference (Cα-only to decrease the overhead from structural alignment at each frame), and the force constant gradually increasing from 10^4 to 5×10^5 kJ/(mol· nm^2) as the target DRMSD decreased from its initial value to ~0.02 nm. From thus obtained initial structures, four enforced rotation simulations were initialized with the γ-shaft angle changing linearly from 60 to 130° over the course of 1 μs (and β-subunit geometries kept in their respective states along a vector connecting the open and closed states in the 3N-dimensional space). The enforced rotation simulations were sampled in 5-degree intervals to generate seeding frames for umbrella sampling, yielding 15 windows, each simulated for 1 μs using the flex2 rotation potential with a force constant of 20 kJ/(mol· nm^2) (52). The Gromacs enforced rotation module (52) and the DRMSD collective variable implemented in Plumed (53) were used to drive the systems to desired states. The free-energy profiles were obtained using the pymbar implementation of the multistate Bennet acceptance ratio (mBAR) method (54). The convergence plots for the rotational free-energy profiles are shown in *SI Appendix*, Fig. S3

Conformational Free-Energy Profiles. To determine the changes in the free energy associated with the opening transition of the β_{TP} subunit in the full F$_1$, the $\alpha_3\beta_3$ subcomplex, and the $\alpha\beta$ heterodimer, we used replica-exchange umbrella sampling (REUS) (55). REUS was chosen as the preferred enhanced sampling method across setups because standard umbrella sampling–if seeded from frames extracted from steered MD–can lead to hysteresis. In contrast, exchanges between neighboring "windows" periodically nudge systems toward local equilibrium, accelerating convergence. As a reaction coordinate describing the transition, we used the difference in root mean square deviation (RMSD) to the closed (R_C) and open (R_O) conformational states (ΔRMSD $= R_C - R_O$), with the crystal structure β_{TP} and β_E taken as the reference closed and open states, respectively. To limit the computational overhead, only every third Cα atom was used for calculating the RMSDs. In the case of full F$_1$, the

conformational free-energy profile was determined for three angular positions of the γ subunit: 0°, 60°, and 90°. In each case, we used 15 equally spaced REUS windows separated by 0.05 nm along the ΔRMSD dimension. A stationary harmonic potential with a force constant of 10^4 kJ/(mol·nm^2) was used to restrain the systems in each of these windows using the Plumed patch (53). Exchanges between neighboring windows were attempted every 10 ps, with an average success rate that varied from 3 to 8% depending on the system. To restrict sampled conformations to ones relevant to the opening transition, a half-harmonic potential was applied to penalize configurations with R_C and R_O greater than 0.36 nm. In each REUS window, the systems were simulated for at least 1 μs, and the last 500 ns were taken for subsequent analysis. Initial configurations for the US windows were generated during 500-ns steered molecular dynamics simulation in which a moving harmonic potential applied to ΔRMSD coordinate was employed to gradually induce the conformational transition of β from the closed to the open conformation. To obtain the unbiased conformational ensemble, the REUS data were postprocessed using the weighted histogram analysis method (WHAM) with the free-energy uncertainties estimated by bootstrap analysis (56). To facilitate interpretation of the results by avoiding divergent free energies around ΔRMSD values corresponding to the reference conformations, the final free-energy profiles were obtained by projecting the unbiased ensemble on the vector connecting the centers of the closed and open states of β in the space spanned by positions of all Cα atoms.

Free-Energy Sensitivity Analysis. To estimate the relative contribution of individual residues to the rotational free-energy profiles, we calculated the derivative of these free-energy profiles with respect to the charge and atom size of selected residues (both generically denoted as σ in the explanation below). By setting up a modified topology in which the coupling parameter λ defines the linear change of σ from σ_A to σ_B, one can obtain the values of $\frac{\partial H}{\partial \sigma}$ as $(\sigma_B - \sigma_A)^{-1} \frac{\partial H}{\partial \lambda}$, where the latter derivative with respect to λ is easily available from the Gromacs free-energy code. Subsequently, the values of $\frac{\partial G_{\theta_0}}{\partial \sigma}$ are estimated as $\langle \frac{\partial H}{\partial \sigma} \rangle|_{\theta=\theta_0}$, where $\langle \rangle$ denotes the average over a trajectory corresponding to the rotation angle θ_0.

By computing and subtracting the derivatives for 60° and 90°, one can estimate the impact of an individual residue on the 60°→90° substep in F$_1$ rotation:

$$\Delta g_\sigma = \frac{\partial G_{90°}(\sigma)}{\partial \sigma} - \frac{\partial G_{60°}(\sigma)}{\partial \sigma}.$$

Note that these derivatives represent only a local response of the free energy to an infinitesimal change in σ; hence, they do not have to correspond to a finite change, e.g., due to mutation.

To unify and simplify the results for atomic charges, we applied this methodology to the absolute value of the charge. This means that, for both positively and negatively charged atoms, the derivative indicates the change of value upon its further charging. Residues with a negative value of Δg_σ promote 60°→90° rotation when their parameter σ increases. For example, if a charge of a given residue is increased and $\Delta g < 0$, then this residue electrostatically promotes rotation. Analogously, if atom sizes of a given residue are increased and $\Delta g > 0$, then this residue sterically impedes rotation. This differentiation algorithm, called ThermoDiff, is implemented in the Python package Gromologist (57).

Author affiliations: [a]Department of Physical Chemistry, Gdansk University of Technology, Gdańsk 80-233, Poland; [b]Department of Theoretical and Computational Biophysics, Max Planck Institute for Multidisciplinary Sciences, Göttingen 37077, Germany; and [c]BioTechMed Center, Gdansk University of Technology, Gdańsk 80-233, Poland

1. P. D. Boyer, The ATP synthase–a splendid molecular machine. *Annu. Rev. Biochem.* **66**, 717–749 (1997).
2. W. Junge, N. Nelson, ATP synthase. *Annu. Rev. Biochem.* **84**, 631–657 (2015).
3. J. P. Abrahams, A. G. Leslie, R. Lutter, J. E. Walker, Structure at 2.8 A resolution of F$_1$-ATPase from bovine heart mitochondria. *Nature* **370**, 621–628 (1994).
4. H. Guo, S. A. Bueler, J. L. Rubinstein, Atomic model for the dimeric FO region of mitochondrial ATP synthase. *Science* **358**, 936–940 (2017).
5. H. Noji, R. Yasuda, M. Yoshida, K. Kinosita, Direct observation of the rotation of F$_1$-ATPase. *Nature* **386**, 299–302 (1997).
6. M. Diez *et al.*, Proton-powered subunit rotation in single membrane-bound F0F1-ATP synthase. *Nat. Struct. Mol. Biol.* **11**, 135–141 (2004).
7. K. Kinosita Jr, K. Adachi, H. Itoh, Rotation of F$_1$-ATPase: How an ATP-driven molecular machine may work. *Annu. Rev. Biophys. Biomol. Struct.* **33**, 245–268 (2004).
8. D. Sabbert, S. Engelbrecht, W. Junge, Functional and idling rotatory motion within F$_1$-ATPase. *Proc. Natl. Acad. Sci. U.S.A.* **94**, 4401–4405 (1997).
9. R. Yasuda, H. Noji, M. Yoshida, K. Kinosita, H. Itoh, Resolution of distinct rotational substeps by submillisecond kinetic analysis of F$_1$-ATPase. *Nature* **410**, 898–904 (2001).
10. K. Shimabukuro *et al.*, Catalysis and rotation of F1 motor: Cleavage of ATP at the catalytic site occurs in 1 ms before 40 substep rotation. *Proc. Natl. Acad. Sci. U.S.A.* **100**, 14731–14736 (2003).
11. T. Suzuki, K. Tanaka, C. Wakabayashi, Ei. Saita, M. Yoshida, Chemomechanical coupling of human mitochondrial F$_1$-ATPase motor. *Nat. Chem. Biol.* **10**, 930–936 (2014).
12. R. Kobayashi, H. Ueno, C. B. Li, H. Noji, Rotary catalysis of bovine mitochondrial F$_1$-ATPase studied by single-molecule experiments. *Proc. Natl. Acad. Sci. U.S.A.* **117**, 1447–1456 (2020).
13. S. Volkán-Kacsó, L. Q. Le, K. Zhu, H. Su, R. A. Marcus, Method to extract multiple states in F$_1$-ATPase rotation experiments from jump distributions. *Proc. Natl. Acad. Sci. U.S.A.* **116**, 25456–25461 (2019).
14. R. Yasuda, H. Noji, K. Kinosita Jr, M. Yoshida, F$_1$-ATPase is a highly efficient molecular motor that rotates with discrete 120 steps. *Cell* **93**, 1117–1124 (1998).
15. S. Toyabe, E. Muneyuki, Single molecule thermodynamics of ATP synthesis by F$_1$-ATPase. *N. J. Phys.* **17**, 015008 (2015).
16. Z. H. He, R. Bottinelli, M. A. Pellegrino, M. A. Ferenczi, C. Reggiani, ATP consumption and efficiency of human single muscle fibers with different myosin isoform composition. *Biophys. J.* **79**, 945–961 (2000).
17. R. Watanabe *et al.*, Mechanical modulation of catalytic power on F$_1$-ATPase. *Nat. Chem. Biol.* **8**, 86–92 (2012).
18. S. Furuike *et al.*, Axle-less F$_1$-ATPase rotates in the correct direction. *Science* **319**, 955–958 (2008).
19. T. Uchihashi, R. Iino, T. Ando, H. Noji, High-speed atomic force microscopy reveals rotary catalysis of rotorless F$_1$-ATPase. *Science* **333**, 755–758 (2011).
20. S. Mukherjee, A. Warshel, Electrostatic origin of the mechanochemical rotary mechanism and the catalytic dwell of F$_1$-ATPase. *Proc. Natl. Acad. Sci. U.S.A.* **108**, 20550–20555 (2011).
21. S. Mukherjee, A. Warshel, Dissecting the role of the γ-subunit in the rotary-chemical coupling and torque generation of F$_1$-ATPase. *Proc. Natl. Acad. Sci. U.S.A.* **112**, 2746–2751 (2015).
22. C. Bai, M. Asadi, A. Warshel, The catalytic dwell in ATPases is not crucial for movement against applied torque. *Nat. Chem.* **12**, 1187–1192 (2020).
23. J. Czub, H. Grubmüller, Torsional elasticity and energetics of F$_1$-ATPase. *Proc. Natl. Acad. Sci. U.S.A.* **108**, 7408–7413 (2011).
24. Ki. Okazaki, G. Hummer, Elasticity, friction, and pathway of γ-subunit rotation in FoF1-ATP synthase. *Proc. Natl. Acad. Sci.* **112**, 10720–10725 (2015).
25. Ki. Okazaki, G. Hummer, Phosphate release coupled to rotary motion of F$_1$-ATPase. *Proc. Natl. Acad. Sci U.S.A.* **110**, 16468–16473 (2013).
26. R. A. Böckmann, H. Grubmüller, Nanoseconds molecular dynamics simulation of primary mechanical energy transfer steps in F$_1$-ATP synthase. *Nat. Struct. Mol. Biol.* **9**, 198–202 (2002).
27. J. Pu, M. Karplus, How subunit coupling produces the γ-subunit rotary motion in F$_1$-ATPase. *Proc. Natl. Acad. Sci.* **105**, 1192–1197 (2008).
28. J. Czub, H. Grubmüller, Rotation triggers nucleotide-independent conformational transition of the empty β subunit of F$_1$-ATPase. *J. Am. Chem. Soc.* **136**, 6960–6968 (2014).
29. K. Nam, J. Pu, M. Karplus, Trapping the ATP binding state leads to a detailed understanding of the F$_1$-ATPase mechanism. *Proc. Natl. Acad. Sci. U.S.A.* **111**, 17851–17856 (2014).
30. A. Singharoy, C. Chipot, M. Moradi, K. Schulten, Chemomechanical coupling in hexameric protein-protein interfaces harnesses energy within V-type ATPases. *J. Am. Chem. Soc.* **139**, 293–310 (2017).
31. J. Czub, M. Wieczor, B. Prokopowicz, H. Grubmüller, Mechanochemical energy transduction during the main rotary step in the synthesis cycle of F$_1$-ATPase. *J. Am. Chem. Soc.* **139**, 4025–4034 (2017).
32. M. Sobti, H. Ueno, H. Noji, A. G. Stewart, The six steps of the complete F$_1$-ATPase rotary catalytic cycle. *Nat. Commun.* **12**, 1–10 (2021).
33. H. Yagi *et al.*, Stepwise propagation of the ATP-induced conformational change of the F$_1$-ATPase β subunit revealed by NMR. *J. Biol. Chem.* **284**, 2374–2382 (2009).
34. J. Hoek, D. Nicholls, J. Williamson, Determination of the mitochondrial protonmotive force in isolated hepatocytes. *J. Biol. Chem.* **255**, 1458–1464 (1980).
35. Y. Kikuchi *et al.*, Thermodynamic analyses of nucleotide binding to an isolated monomeric β subunit and the $\alpha3\beta3\gamma$ subcomplex of F$_1$-ATPase. *Biophys. J.* **105**, 2541–2548 (2013).
36. K. Y. Hara *et al.*, The role of the delseed motif of the β subunit in rotation of F$_1$-ATPase. *J. Biol. Chem.* **275**, 14260–14263 (2000).
37. D. Arsenieva, J. Symersky, Y. Wang, V. Pagadala, D. M. Mueller, Crystal structures of mutant forms of the yeast F$_1$-ATPase reveal two modes of uncoupling. *J. Biol. Chem.* **285**, 36561–36569 (2010).
38. Y. Wang, U. Singh, D. M. Mueller, Mitochondrial genome integrity mutations uncouple the yeast Saccharomyces cerevisiae ATP synthase. *J. Biol. Chem.* **282**, 8228–8236 (2007).
39. M. Tanigawara *et al.*, Role of the DELSEED loop in torque transmission of F$_1$-ATPase. *Biophys. J.* **103**, 970–978 (2012).
40. K. Adachi, K. Oiwa, M. Yoshida, T. Nishizaka, K. Kinosita, Controlled rotation of the F$_1$-ATPase reveals differential and continuous binding changes for ATP synthesis. *Nat. Commun.* **3**, 1–12 (2012).
41. T. Masaike, F. Koyama-Horibe, K. Oiwa, M. Yoshida, T. Nishizaka, Cooperative three-step motions in catalytic subunits of F$_1$-ATPase correlate with 80 and 40 substep rotations. *Nat. Struct. Mol. Biol.* **15**, 1326–1333 (2008).
42. H. Wang, G. Oster, Energy transduction in the F1 motor of ATP synthase. *Nature* **396**, 279–282 (1998).
43. S. Sun, D. Chandler, A. R. Dinner, G. Oster, Elastic energy storage in β-sheets with application to F$_1$-ATPase. *Eur. Biophys. J.* **32**, 676–683 (2003).
44. S. Volkán-Kacsó, R. A. Marcus, *Single Molecule Studies of a Biological Motor F$_1$-ATPase: Interplay of Experiment, Analytic Theory and Computation in Computational Materials, Chemistry, and Biochemistry: From Bold Initiatives to the Last Mile* (Springer, 2021), pp. 927–933.
45. J. Gledhill, M. Montgomery, A. Leslie, J. Walker, Mechanism of inhibition of bovine F$_1$-ATPase by resveratrol and related polyphenols. *Proc. Natl. Acad. Sci. U.S.A.* **104**, 13632–7 (2007).
46. C. Gibbons, M. G. Montgomery, A. G. Leslie, J. E. Walker, The structure of the central stalk in bovine F$_1$-ATPase at 2.4 å resolution. *Nat. Struct. Biol.* **7**, 1055–1061 (2000).
47. J. Huang, A. D. Mackerell, CHARMM36 all-atom additive protein force field: Validation based on comparison to NMR data. *J. Comput. Chem.* **34**, 2135–2145 (2013).
48. B. Hess, H. Bekker, H. Berendsen, J. Fraaije, LINCS: A linear constraint solver for molecular simulations. *J. Comput. Chem.* **18** (1998).
49. S. Miyamoto, P. A. Kollman, Settle: An analytical version of the SHAKE and RATTLE algorithm for rigid water models. *J. Comput. Chem.* **13**, 952–962 (1992).
50. T. Darden, D. York, L. Pedersen, Particle mesh Ewald: An N·log(N) method for Ewald sums in large systems. *J. Chem. Phys.* **98**, 10089–10092 (1993).
51. M. J. Abraham *et al.*, Gromacs: High performance molecular simulations through multi-level parallelism from laptops to supercomputers. *SoftwareX* **1–2**, 19–25 (2015).
52. C. Kutzner, J. Czub, H. Grubmüller, Keep it flexible: Driving macromolecular rotary motions in atomistic simulations with GROMACS. *J. Chem. Theory Comput.* **7**, 1381–1393 (2011).
53. G. A. Tribello, M. Bonomi, D. Branduardi, C. Camilloni, G. Bussi, PLUMED 2: New feathers for an old bird. *Comput. Phys. Commun.* **185**, 604–613 (2014).
54. M. R. Shirts, J. D. Chodera, Statistically optimal analysis of samples from multiple equilibrium states. *J. Chem. Phys.* **129**, 124105 (2008).
55. Y. Sugita, A. Kitao, Y. Okamoto, Multidimensional replica-exchange method for free-energy calculations. *J. Chem. Phys.* **113**, 6042–6051 (2000).
56. S. Kumar, J. M. Rosenberg, D. Bouzida, R. H. Swendsen, P. A. Kollman, THE weighted histogram analysis method for free-energy calculations on biomolecules I. The method. *J. Comput. Chem.* **13**, 1011–1021 (1992).
57. M. Wieczor, J. Czub, Gromologist: A gromacs-oriented utility library for structure and topology manipulation. ChemRxiv, 1–5 (2022).